Negative pressure driven phase transformation in Sr doped $SmCoO_3$

2010 J. Phys.: Condens. Matter 22 075402

(http://iopscience.iop.org/0953-8984/22/7/075402)

J. Phys.: Condens. Matter **22** (2010) 075402 (9pp) doi:10.1088/0953-8984/22/7/075402

Negative pressure driven phase transformation in Sr doped $SmCoO_3$

M Arshad Farhan and M Javed Akhtar[1]

Physics Division, PINSTECH, PO Nilore, Islamabad 1482, Pakistan

E-mail: javeda@pinstech.org.pk

Received 28 September 2009, in final form 9 December 2009
Published 2 February 2010
Online at stacks.iop.org/JPhysCM/22/075402

Abstract

Atomistic computer simulation techniques based on energy minimization procedures are utilized for the structural investigation of perovskite-type $SmCoO_3$. A reliable potential model is derived which reproduces both cubic as well as orthorhombic phases of $SmCoO_3$. We observe a negative chemical pressure induced structural phase transformation from distorted perovskite (orthorhombic) to perfect perovskite (cubic) due to the substitution of Sr^{2+} at the Sm^{3+} sites. However, external hydrostatic pressure shows isotropic compression and no pressure-induced structural transformation is observed up to 100 GPa. To maintain the electroneutrality of the system, charge compensation is through oxygen vacancies which results in the brownmillerite-type structure. A defect model is proposed, which is consistent with experimental results. The solution energies for divalent and trivalent cations are also calculated. These results show that the cations having ionic radii less than 0.75 Å will occupy the Co sites and those with ionic radii larger than 0.75 Å will substitute at the Sm sites.

(Some figures in this article are in colour only in the electronic version)

1. Introduction

Perovskite (ABO_3)-type rare earth cobaltites have attracted a great deal of interest for some time due to their remarkably unique properties. Most of the studies are focused on the $LnCoO_3$ (where Ln = La, Nd, Sm, etc) system. These materials show novel characteristics such as magnetic susceptibility [1, 2], metal–insulator transition [3–6], complex electronic structure [7, 8] and temperature dependence of magnetic properties [9]. $SmCoO_3$ is an important member of the cobaltites family due to its excellent gas sensing abilities [10, 11], low temperature magnetic behaviour [12], giant magnetoresistance [13] and applications in direct methanol fuel cells (DMFC) and proton exchange membrane fuel cells (PEMFC) as electrodes [14]. Doping of a divalent ion such as Sr^{2+} results in enhanced electrical and ionic conductivities along with better optical properties [15, 16]. However, a diverse opinion exists regarding its structure and physical properties. A structural phase transition from orthorhombic ($SmCoO_3$) to brownmillerite-type ($Sr_2Co_2O_5$) arrangement, with cubic symmetry, has been observed [16, 17].

The doping and pressure can affect the electrical, magnetic, transport and structural properties of the materials in identical manners in many respects [18–22]. The application of high pressure changes the interatomic distances (lattice parameters) which intimately control the physical properties. Analogous to the external pressure, dopants can change the lattice parameters by chemical pressure; if the dopant has smaller ionic radius than the host atom, this can cause a reduction in the lattice parameter. In contrast, if the ionic radius of a dopant is larger than the host cation, then lattice parameters may increase due to negative chemical pressure. The isostructural phase transitions have been predicted in perovskites theoretically by applying negative hydrostatic pressure, which is not viable experimentally [23, 24]. However, the influence of positive pressure (compression of lattice) and negative pressure (expansion of lattice) may provide useful insights into the structural instabilities, which are valuable to improve the existing properties of novel materials.

Static simulation techniques based on energy minimization procedures are among the various methods utilized by the scientific community to investigate the structural properties of crystalline materials. These methods have been used

[1] Author to whom any correspondence should be addressed.

to investigate the effects of different dopants on parent materials [25–28] as well as the effects of high pressure on structural parameters [29–31]. In order to investigate the effects of chemical pressure, due to substitution of dopant cations, and external hydrostatic pressure on the lattice parameters of $SmCoO_3$, we have employed static simulation techniques. First a potential model is derived which can reproduce both orthorhombic and cubic structures of $SmCoO_3$, and then the effects of chemical pressure and hydrostatic pressure are investigated. The selection of Sr as a dopant has twofold interests: firstly, as has been indicated earlier [15, 16] Sr affects the various properties of $SmCoO_3$. Secondly, Sr^{2+} has an ionic size larger than both Sm^{3+} and Co^{3+}, hence it can cause the lattice to expand, i.e. it can create negative chemical pressure. The structure of $SmCoO_3$ has also been simulated under external hydrostatic pressure up to 100 GPa. In the final part, we will investigate various divalent and trivalent cations as dopants and explore different modes of substitution in $SmCoO_3$ and their effects on the structural parameters.

2. Simulation methodology

Static simulation techniques employed in the present study are based on energy minimization methods, without considering any thermal motion within the material. The methodology had been described in detail elsewhere [29, 32, 33]; here we present only a brief description of these techniques. The basis of these calculations is the specification of a potential model, which describes the potential energy of the system as a function of atomic coordinates and allows evaluation of the lattice energy. For ceramic oxides, the Born model provides the framework for simulating the system describing the crystal as composed of discrete ions with integral charges, taking into consideration both the attractive and repulsive forces. The general expression for the lattice energy of any solid is generally represented as

$$E_{\mathrm{L}} = \sum_{ij} \frac{q_i q_j}{4\pi\varepsilon_{\mathrm{o}} r_{ij}} + \sum_{ij} E_{(i,j)} + \sum_{ijk} E_{(i,j,k)} + \cdots. \quad (1)$$

The summations refer to all pairs of ions i, j and triplets of ions i, j and k in the crystal. In principle, terms involving larger numbers of ions could be included; but for ionic solids it is rare to take the summations beyond the three-body terms. The first term on the right-hand side of equation (1) is the long range (Coulombic) interaction, where q_i and q_j are the charge of ions i and j separated by interatomic distance r_{ij} and ε_0 is the permittivity. The short range interactions between a pair of ions are described by an analytical function of the Buckingham form:

$$E_{ij}(r_{ij}) = A_{ij} \exp\left(-\frac{r_{ij}}{\rho_{ij}}\right) - \frac{C_{ij}}{r_{ij}^6}. \quad (2)$$

The interactions, A_{ij} and ρ_{ij}, are the potential parameters describing the repulsive forces while C_{ij} is of the attractive nature. These parameters are derived empirically for each ion–ion interaction by employing the least-squares fitting procedures, so that the difference between observed and calculated properties is minimized.

Defects in ionic crystals are charged species and will polarize other ions in the lattice; therefore, ionic polarizability must be accounted for in these calculations. This can be achieved by incorporating the shell model [34], which treats each ion in terms of a core (representing the nucleus and core electrons) connected to a massless shell (representing valence electrons having charge Y) via a harmonic spring constant k. The free ion polarizability, α, may be written as

$$\alpha = \frac{Y^2}{k}. \quad (3)$$

Variations in lattice parameters with Sr concentrations are calculated by employing a *partial occupancy mean field* strategy [35]. The ions are considered to be randomly distributed in the solid solution, which causes each site to experience a potential, which is the mean of all possible configurations on the disordered positions maintaining the overall crystal symmetry during the ion relaxations; further details are described elsewhere [25]. Defect calculations are employed by considering the Mott–Littleton approach [36] which involves partitioning the crystal lattice into two regions. The inner region, which surrounds the defect, contains 200–300 ions and is relaxed explicitly, while the remainder of the crystal, where defect forces are relatively weak, is treated by a more approximate quasi-continuum approach [32].

Any impurity ion causes a strain in the lattice which is subsequently relaxed by displacing the constituting entities in three dimensions. External pressure therefore acts in a way quite similar to the substitution of an impurity ion in the lattice. For an isotropic material the pressure, P, is simply the derivative of the free energy, F, with respect to volume, V, and is given by

$$P = \frac{\mathrm{d}F}{\mathrm{d}V}. \quad (4)$$

The pressure is determined by calculating the free energy at a given volume and then recalculating after making a small adjustment to the cell volume, $\mathrm{d}V$. In the case of non-cubic materials the problem is relatively more complicated as the change in volume will not be isotropic. For these systems we have to consider six different strain components, ε_j. However, the same approach is used but with a small strain applied in each of the six directions, and the kinetic pressure corresponding to the derivative of the free energy for each component is given by

$$P_j = \frac{1}{V}\frac{\mathrm{d}F}{\mathrm{d}\varepsilon_j}. \quad (5)$$

Further details of high pressure simulation techniques are given by Parker and Price [29]. These methodologies are embodied in the general utility lattice program (GULP) [37] which has been used for all calculations in this work.

3. Results and discussion

3.1. Interatomic potentials

The interatomic potentials play a key role in computer simulations; therefore, it is necessary to have reliable potential

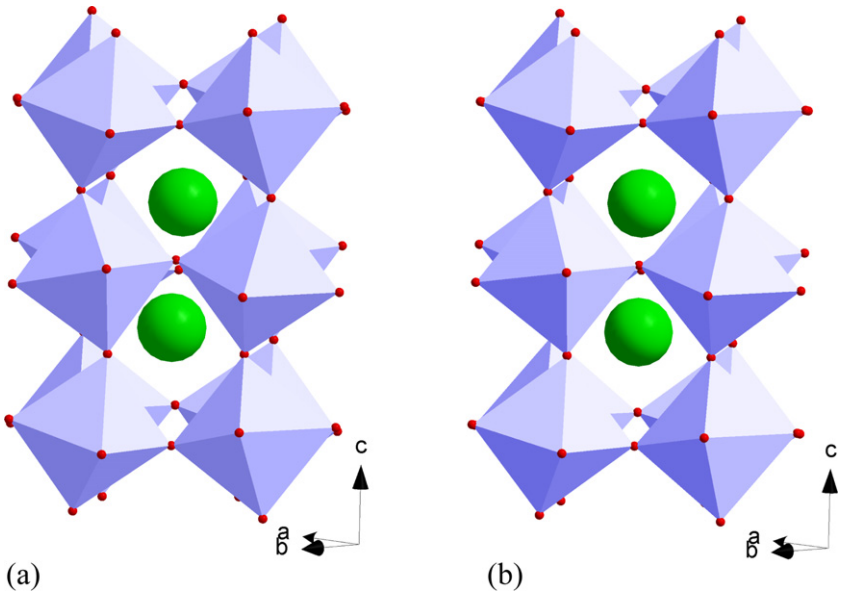

Figure 1. Simulated orthorhombic crystal structure of $SmCoO_3$ (a) before relaxation and (b) after relaxation; corner-sharing octahedra denote CoO_6 with Sm residing in the centre.

parameters for $SmCoO_3$. In the present study, we took initial parameters from $LaCoO_3$ (as both materials are isostructural). The Co^{3+}–O^{2-} and O^{2-}–O^{2-} interactions parameters were kept the same as in the previous study [28], whereas the Sm^{3+}–O^{2-} potential parameters were derived by simultaneous optimization of both orthorhombic and cubic phases of $SmCoO_3$. To the best of our knowledge, no other structural properties like the elastic constants and dielectric constants of $SmCoO_3$ are available; therefore only crystal structures are used for the optimization of potential parameters. The Sm^{3+}–O^{2-} potential parameters were also checked to reproduce the structural properties of Sm_2O_3. By using this potential, to generate the structure of Sm_2O_3, a lattice parameter of 10.84 Å is obtained which is in good agreement with the experimental values of 10.94 Å [38]. The final potential parameters for $SmCoO_3$ are given in table 1. The calculated properties of $SmCoO_3$ and Sm_2O_3 are given in table 2. For dopant ions the potential parameters are taken from [39].

Table 1. Interatomic potential parameters used for simulation of $Sm_{1-x}Sr_xCoO_3$.

(a) Short range interactions (potential cutoff = 12 Å)			
Interaction	A (eV)	ρ (Å)	C (eV Å^6)
Sm^{3+}–O^{2-}	1 297.797	0.3609	0.00
Co^{3+}–O^{2-}	1 329.82	0.3087	0.00
Sr^{2+}–O^{2-}	959.70	0.3721	0.00
O^{2-}–O^{2-}	22 764.30	0.149	43.00
(b) Shell model			
Entity	Y (e)	k (eV Å^{-2})	
Sm^{3+}	−0.250	150	
Co^{3+}	2.040	196.3	
Sr^{2+}	3.251	71.7	
O^{2-}	−2.389	42	

3.2. Unit cell parameters

It has been reported that $SmCoO_3$ exists in two different crystal structures, i.e. orthorhombic (*Pbnm*) [16, 40] and cubic (*Pm3m*) [38, 41, 42] forms. As mentioned above, both structures were simultaneously used to optimize the potential model. During the energy minimization process, fitting was started with the reported experimental structure to avoid trapping in some local minima in the geometric space. For cubic, the final lattice parameter obtained is 3.773 Å, which is in good agreement with the reported value of 3.750 Å [38, 41, 42]. In the present study, for the cubic phase Co is placed at 1a sites (0, 0, 0), Sm at 1b sites (1/2, 1/2, 1/2) and oxygen at 3d sites (1/2, 0, 0). For the orthorhombic phase, the initial structural parameters are taken from Pérez-Cacho *et al* [40]. In table 3, we compare the final simulated structural parameters with experimental results; we observe a good agreement between simulated and experimental results. Figures 1(a) and (b) show the unrelaxed and relaxed structures of the orthorhombic phase, where distortion of the corner sharing octahedra (representing CoO_6) is visible. However, for the cubic phase perfect octahedra are observed as shown in figure 2. The calculated lattice energies for the cubic and orthorhombic phases are −144.40 eV and −144.54 eV, respectively. This small difference in lattice energy (0.14 eV) indicates that $SmCoO_3$ can exist in both cubic and orthorhombic phases [JCPDF nos. 75-0282 and 25-1071].

3.3. Preferable substitution site for a dopant ion in $SmCoO_3$

We have considered divalent and trivalent cations as dopants in $SmCoO_3$, in principle these dopants can substitute either at the Sm or Co sites. The trivalent cations are isovalent, whereas divalent dopants create extra negative charge on the

Table 2. Calculated properties of cubic and orthorhombic phases of $SmCoO_3$ and Sm_2O_3.

Property	Cubic $SmCoO_3$	Orthorhombic $SmCoO_3$	Sm_2O_3
Lattice energy (eV/f.u.)	−144.40	−144.54	−131.20
Dielectric constants			
Static (ε^o)			
x	65.24	20.08	10.89 (13.93)[a]
y		25.62	
z		24.84	
High frequency (ε^∞)			
x	2.40	2.41	1.96
y		2.41	
z		2.41	
Elastic constants (dyn $cm^{-2} \times 10^{11}$)			
C_{11}	44.38	47.97	23.45
C_{22}	44.38	43.07	23.45
C_{33}	44.38	40.76	23.45
C_{44}	17.23	17.87	8.57
C_{55}	17.23	17.35	8.57
C_{66}	17.23	11.25	8.57
C_{12}	17.23	12.74	11.18
C_{13}	17.23	18.77	11.18
Young's modulus (GPa)			
x	347.40	387.38	162.31
y		348.35	
z		293.32	
Bulk modulus (GPa)	262.78	255.20	152.74

[a] The values in brackets are the calculated results taken from [51].

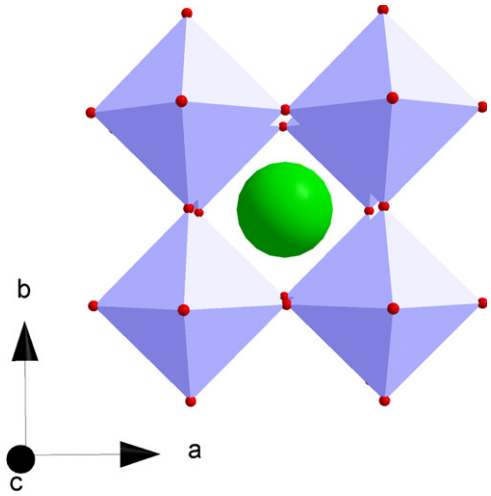

Figure 2. Simulated cubic crystal structure of $SmCoO_3$ after relaxation, c axis points out of the paper plane; corner-sharing octahedra denote CoO_6 with Sm residing in the centre.

Table 3. Comparison of simulated and experimental [39] structural parameters of orthorhombic $SmCoO_3$.

Lattice parameters		Experimental	Simulated
a (Å)		5.2831	5.3398
b (Å)		5.3502	5.3563
c (Å)		7.4962	7.5552
Cell volume ($Å^3$)		211.880	216.093
Sm 4c sites	x	0.9908	0.9982
	y	0.0467	0.0165
Co 4b sites	—	—	—
O(I) 4c sites	x	0.0830	0.0579
	y	0.4880	0.4850
O(II) 8d sites	x	0.7080	0.7178
	y	0.2890	0.2816
	z	0.0392	0.0299

lattice, which can be compensated by oxygen vacancies or by the formation of a hole. The two equations representing the defect models, based on the thermodynamics considerations, can be written as follows:

$$XO + M_M + O_O \leftrightarrow X'_M + \tfrac{1}{2}V_O^{\bullet\bullet} + \tfrac{1}{2}M_2O_3 \quad (6)$$

$$XO + M_M + \tfrac{1}{4}O_{2(g)} \leftrightarrow X'_M + h^\bullet + \tfrac{1}{2}M_2O_3, \quad (7)$$

where XO signifies the dopant oxide and M represents the host cation (Sm or Co). The hole formation can take place on either of the three constituting entities, i.e. Sm^{3+}, Co^{3+} or O^{2-}; our calculations reveal that the hole formation is energetically more favourable at O^{2-} as compared to the hole formation on Co^{3+} or Sm^{3+}. However, oxygen vacancy is the most favourable process for charge compensation for divalent dopants in $SmCoO_3$. We will discuss substitution of divalent and trivalent dopants in detail at a later stage.

A number of studies have been carried out to investigate the influence of internal pressure generated by mismatch of the ionic size of the dopant to that of the host ion in various perovskites [43–46]. When there is mismatch between host and dopant cations, the Goldschmidt [47] tolerance factor is considered as an indicator to identify the lattice site. The

Table 4. Bond distance (Å) as a function of Sr concentration.

	0%	10%	20%	30%	40%	50%	60%	70%	80%	90%	100%
Sm–O1	2.376	2.406	2.432	2.479	2.540	2.697	2.698	2.698	2.695	2.691	2.684
Sm–O1	2.530	2.591	2.673	2.700	2.700						
Sm–O1	2.865	2.806	2.730	2.703	2.701						
Sm–O1	2.974	2.949	2.930	2.894	2.844						
Sm–O2 (2)	2.383	2.420	2.492	2.546	2.591	2.692	2.699				
Sm–O2 (2)	2.649	2.609	2.541	2.550	2.592						
Sm–O2 (2)	2.650	2.716	2.818	2.824	2.788	2.693					
Sm–O2 (2)	3.053	2.993	2.891	2.829	2.789						
Co–O1(2)	1.916	1.917	1.918	1.913	1.907	1.908	1.908	1.918	1.931	1.947	1.967
Co–O2(2)	1.918	1.912	1.908	1.908	1.908						
Co–O2(2)	1.921	1.914	1.909								
O1–O1(2)	3.374	3.392	3.412	3.477	3.568	3.801	3.816	3.815	3.811	3.805	3.796
O1–O1(2)	3.831	3.834	3.836	3.825	3.813	3.813					
O1–O2 (2)	2.691	2.691	2.695	2.698	2.696	3.816	2.699	2.705	2.713	2.722	2.733
O1–O2 (2)	2.692	2.701	2.701	2.699							
O1–O2 (2)	2.731	2.714	2.710	2.705	2.699	2.692					
O1–O2 (2)	2.733	2.727	2.717	2.747							
O1–O2	2.691	2.691	2.695	2.698	2.696	2.696					
O1–O2	2.692	2.701	2.701	2.699							
O1–O2	2.731	2.714	2.710	2.705	2.699						
O1–O2	2.733	2.727	2.717	2.705							
O2–O2 (2)	2.700	2.690	2.683	2.688	2.693	2.697					
O2–O2 (2)	2.729	2.722	2.715	2.709	2.703						
O2–O2	3.325	3.344	3.368	3.446	3.551	3.800	3.816	3.815	3.812	3.805	3.796
O2–O2	3.330	3.480	3.730	3.810	3.815	3.802					
O2–O2	3.836	3.824	3.816	3.816	3.816	3.814					
O2–O2	3.842	3.829	3.818	3.822	3.816	3.815					

Goldschmidt tolerance factor is given by

$$t = \frac{r_A + r_O}{\sqrt{2}(r_B + r_O)}, \tag{8}$$

where r_A is the ionic radius of A, r_B is the ionic radius of B and r_O is the ionic radius of oxygen. The ionic radii of ions depend on the valence state and coordination numbers [48]. The tolerance factor can be used to calculate the lattice site for a dopant ion. For an ideal perovskite, the tolerance factor should be close to unity: hence, for a dopant ion the preferable site in the lattice is that where the tolerance factor is close to 1. The tolerance factor calculated for $SmCoO_3$ is 0.964, which is in excellent agreement with the reported value of 0.966 [42]. For doping of Sr at the A (Sm) site the tolerance factor is 1.038, whereas, for the B (Co) site substitution it is 0.724. Hence, from these results we can infer that Sr will substitute at the Sm sites. These results are in agreement with our thermodynamics calculations where we found that for Sr^{2+} ion it is 4.5 eV energetically more favourable to substitute at the Sm^{3+} sites than Co^{3+} sites and extra negative charge is compensated by the oxygen vacancies.

3.4. Effects of Sr^{2+} doping on lattice parameters

In the present study we investigate in detail the effects of Sr^{2+} doping on the crystal structure of $SmCoO_3$. As we have already mentioned when $SmCoO_3$ is doped with a divalent cation (like Sr^{2+}) electroneutrality of the system is maintained by the oxygen vacancy compensation mechanism. Variations in bond lengths of the constituting entities as a function of Sr^{2+} concentration are given in table 4. We note that, as concentration of Sr is increased, the system moves from low symmetry to high symmetry and at 60% Sr concentration, all bond lengths between samarium–oxygen, cobalt–oxygen and oxygen–oxygen show cubic structure formation. The Jahn–Teller distortion of CoO_6 observed in octahedral symmetry is suppressed with the increase in the Sr concentration, From table 4 we note that initially CoO_6 octahedra have three pairs of bond lengths which show a complete distortion. When the concentration of Sr is increased to 30%, four bond lengths become equal and two bond lengths are different, indicating tetragonal transformation, which furthermore becomes cubic at 60% Sr doping level, when all six bond lengths become equal, making perfect CoO_6 octahedra of cubic symmetry. This results in the formation of an ideal perovskite structure, which is consistent with the experimental study [16].

Figure 3 shows variation in the lattice parameters of $SmCoO_3$ with Sr doping, where orthorhombic lattice parameters convert into cubic at 60% Sr concentration. We note that lattice parameters increase with increase in the Sr concentration, causing a negative chemical pressure. This increase in the lattice parameter can be attributed to the larger ionic size of Sr^{2+} as compared to the Sm^{3+} ion [48]. In figure 4, we compare our simulated results with the experimental data reported by Tu *et al* [16]; the orthorhombic lattice parameters were converted to pseudocubic lattice parameters using the relations $a_o = c_o = a_c\sqrt{2}$ and $b_o = 2a_c$. We observe a good agreement between experimental and simulated results, although we note that undoped lattice parameters reported by Tu *et al* [16] are different from our starting values, which were taken from [40]. However, both studies show that, up to 50% doping level, the increase in

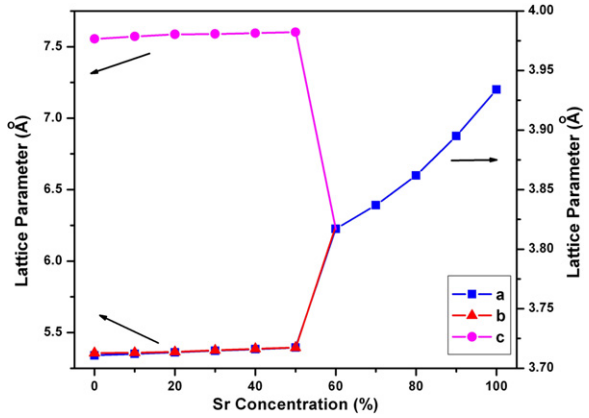

Figure 3. Simulated variation in lattice parameter as a function of Sr concentration.

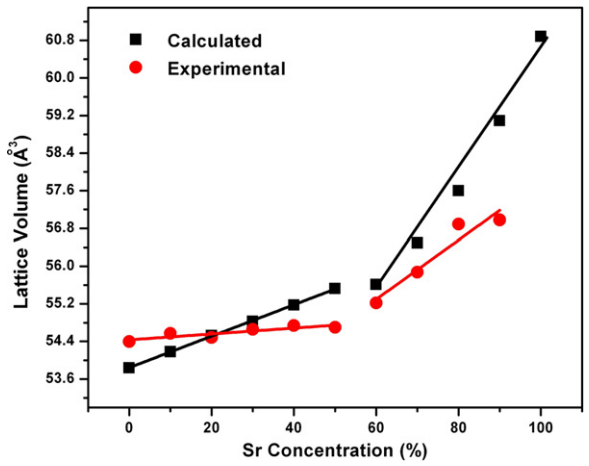

Figure 4. Comparison of simulated and experimentally reported [16] variations in pseudocubic lattice volume as a function of Sr concentration.

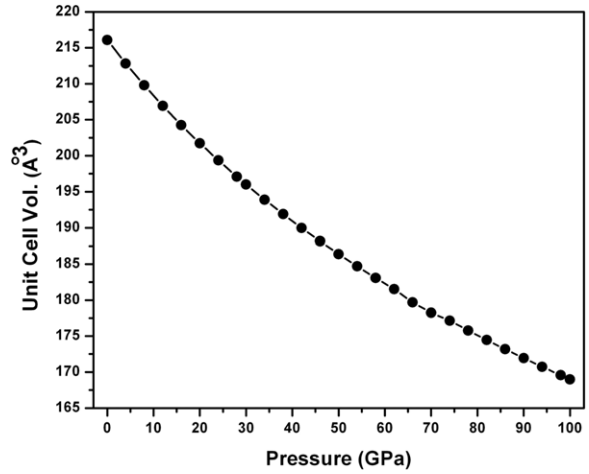

Figure 5. Variation of cell volume with pressure.

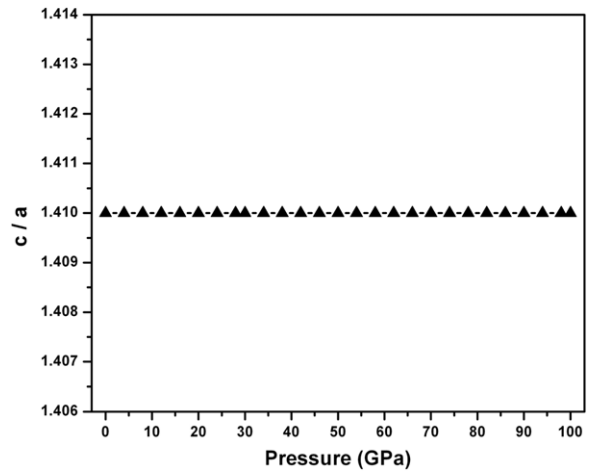

Figure 6. c/a ratio of $SmCoO_3$ with pressure.

volume is relatively low, while above 60% doping level the lattice volume has a much steeper slope, which may be due to transformation from orthorhombic to the brownmillerite-type cubic structure. These results clearly demonstrate that there is a structural phase transformation from distorted perovskite (orthorhombic) to perfect perovskite (cubic), which has originated from a negative chemical pressure on the lattice, due to the substitution of Sr at Sm sites.

3.5. Effect of hydrostatic high pressure

High pressure studies are being employed to investigate and understand the effect of pressure on the physical properties including electronic configuration, magnetic properties and crystal structures [49, 50]. The motivations behind these studies are twofold: firstly, the knowledge of the effect of pressure on these fundamental properties provides a sound base for improving the existing properties and for the synthesis of new materials. Secondly, the understanding of pressure affects help in the formulation of new theories and substantiation of the existing theories of solid state behaviour. In this study we have simulated the structural properties of $SmCoO_3$ under applied external pressure up to 100 GPa. Figure 5 shows the variation of volume with pressure. We note that the unit cell decreases monotonically up to 100 GPa. The c/a ratio, shown in figure 6, gives a straight line in the entire pressure range which implies that external pressure has an isotropic effect on the compressibility of lattice parameters. We have also carried out high pressure studies of the cubic phase, where we observed that the enthalpy of the orthorhombic phase is lower than the enthalpy of the cubic phase at 100 GPa, suggesting that the orthorhombic phase is stable under high hydrostatic pressure. As discussed earlier, the applied external pressure and introduction of impurity (doping) in the parent material affects the lattice parameters in a similar way that both affect the interatomic distances, which can cause contraction or expansion of the lattice parameters. A comparison of the volume compressibility of $SmCoO_3$ with external pressure and Sr concentration (negative chemical pressure) is shown in figure 7. The volume compressibility as a function of pressure decreases gradually with increase in pressure, whereas volume compressibility with Sr concentration shows the opposite trend.

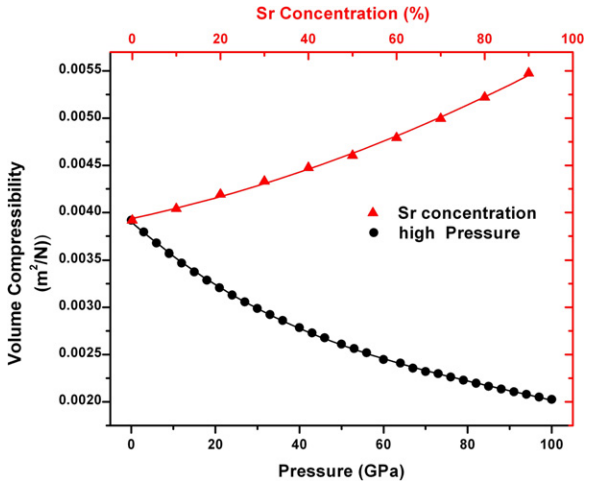

Figure 7. Comparison of volume compressibility of $SmCoO_3$ with pressure and with Sr^{2+} concentration.

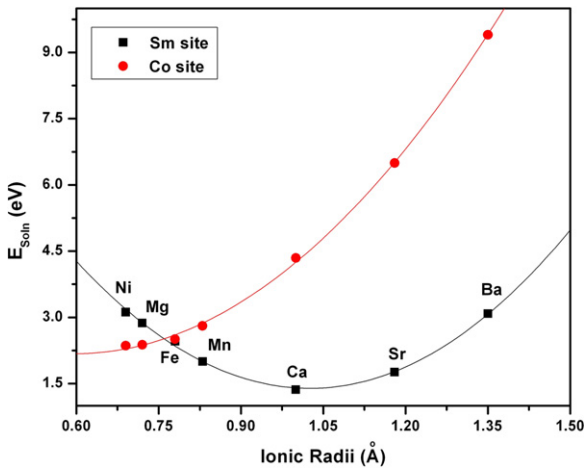

Figure 8. Solution energies for divalent cations in $SmCoO_3$.

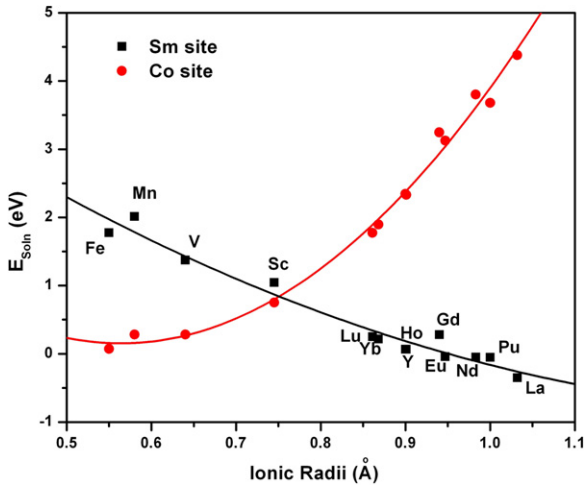

Figure 9. Solution energies for trivalent cations in $SmCoO_3$.

3.6. Substitution of dopants in $SmCoO_3$

The presence of impurity species (dopants) in any material may have profound effects on its electrical, magnetic and structural properties [2, 5, 13, 15, 16]. The mismatch of ionic radii between host and dopant ions can cause an internal strain in the lattice. In addition, when the dopant ion is aliovalent to the host ion, extra defects are required to maintain the charge neutrality of the system. In the present study, we investigate the effects of divalent and trivalent cations on the crystal structure of $SmCoO_3$. As previously discussed, the dopant ions, in principle, can be substituted either at the Sm or Co site. Here we explore which site (Sm or Co) a dopant ion can preferably occupy when substituted in $SmCoO_3$ and what will be the effects of doping on the structural parameters.

Figure 8 shows the solution energies for divalent dopants with ionic radii. It is a well-known fact that ionic radii vary with valence state and coordination numbers [48]; in the case of $SmCoO_3$ both cations have the same charge but different coordination numbers, Co is 6-coordinated while Sm is 12-coordinated. In order to make a simplified comparison, we have plotted all ionic radii for 6-coordinated cations; the ionic radii for 12-coordinated cations are approximately 30% larger than 6-coordinated cations. This implies that Sm site substitution shows a qualitative representation of the solution energies when plotted against ionic radii. For divalent cations solution energies for the Co^{3+} site substitution increase with increase in the ionic radii. However, for the Sm^{3+} site substitution initially solution energy decreases with increase in the ionic radii but after a minimum around 1.0 Å it starts increasing again. We note that both lines cross each other around 0.75 Å, suggesting that cations having ionic radii less than 0.75 Å (mostly transition elements) substitute at the Co^{3+} site while cations having ionic radii larger than 0.75 Å preferentially go to the Sm^{3+} sites. It is interesting to note that Fe^{2+} have almost the same solution energies for both Sm^{3+} and Co^{3+} site substitutions, which indicates that Fe^{2+} can simultaneously substitute at both sites. The ionic radius of Fe^{2+} is larger than Co^{3+}, but smaller than Sm^{3+}. Therefore, the substitution of Fe^{2+} in $SmCoO_3$ is expected to have *self-compensation* effects on the lattice parameters, where increase in lattice parameter due to substitution at the Co^{3+} site is compensated by the decrease in lattice parameter due to the Sm^{3+} site substitution. For Mn^{2+} it is preferable to substitution at the Sm sites; we note that Mn^{2+} is the only divalent cation (in this study) which has an ionic radius smaller than the host cation, which implies that it will cause a contraction (positive pressure effect) in the lattice. The rest of the divalent cations, whether they substitute at the Co sites (like Ni and Mg) or at the Sm sites (like Ca, Sr, Ba) will have a negative chemical pressure effect on the lattice parameters.

Since trivalent ions (M^{3+}) are isovalent to Sm^{3+} and Co^{3+} ions, therefore no charge compensating defects are required. Figure 9 shows variation of the solution energies with ionic radii for trivalent cations. Solution energies for the Sm site substitution decrease linearly with increase in the ionic radii, whereas solution energies increase with the second-order polynomial for the Co site substation. We note that the two fitted lines cross each other around 0.75 Å, which shows that trivalent cations having ionic radii smaller than this will

substitute at the Co sites while those having ionic radii larger than 0.75 Å will preferably substitute at the Sm sites. The solution energy for substitution of Sc at the Co site is slightly lower than the Sm site substitution, suggesting that it has very small preference to substitute at the Co site, whereas at higher temperature it can substitute at the Sm site as well. We can also predict that cations (like Lu, Yb) having ionic radii smaller than Sm may exert positive pressure effects on the lattice, while the cations having larger ionic radii (like Pu and La) will have negative chemical pressure effects. However, it is anticipated that cations like Nd and Eu having ionic radii close to Sm will not affect the lattice parameters by appreciable amounts.

4. Conclusions

In the present study we have derived a potential model which can reproduce both orthorhombic and cubic phases of $SmCoO_3$. The calculated results reveal that the lattice energies of $SmCoO_3$ for both structures (i.e. orthorhombic and cubic) are very close, suggesting the existence of both phases. We have investigated the effects of Sr doping on the structural parameters of $SmCoO_3$ and it is observed that Sr substitutes at the Sm sites with oxygen vacancies as the charge compensating species. In addition, it is noticed that there is a negative chemical pressure driven phase transformation from the orthorhombic to the cubic symmetry at 60% doping level. However, application of external pressure shows that there is an isotropic compression and no structural phase instability is observed up to 100 GPa.

In the case of divalent dopants, we observed that cations having ionic radii less than 0.75 Å substitute at the Co^{3+} site while cations having ionic radii larger than 0.75 Å preferably go to the Sm^{3+} sites. However, Fe^{2+} can simultaneously substitute at both Sm^{3+} and Co^{3+} sites; and due to *self-compensation* characteristics, it is not expected to have any significant effect on the lattice parameters. For divalent cation substitution, the extra negative charge on the lattice is compensated by oxygen vacancies, which results in the brownmillerite-type structure.

Trivalent cations having ionic radii below 0.75 Å will substitute at the Co^{3+} sites while those having ionic radii larger than 0.75 Å will substitute at the Sm^{3+} sites. Trivalent dopants substituting at the Sm^{3+} sites are anticipated to have three types of effects on the lattice parameters. Those having ionic radii larger than Sm have negative chemical pressure effects (expansion of the lattice), while those having ionic radii smaller than Sm will have positive pressure effects (contraction of the lattice), whereas cations having ionic radii close to that of Sm are not expected to cause any type of distortions in the lattice.

References

[1] Zobel C, Kriener M, Bruns D, Baier J, Gruninger M and Lorenz T 2002 *Phys. Rev.* B **66** 020402
[2] Caciuffo R, Rinaldi D, Barucca G, Mira J, Rivas J, Senaris-Rodrigues M A, Radaelli P G, Fiorani D and Goodenough J B 1999 *Phys. Rev.* B **59** 1068
[3] Thornton G, Morrison F C, Partington S, Tofield B C and Williams D E 1988 *J. Phys. C: Solid State Phys.* **21** 2871
[4] Tokura Y, Okimoto Y, Yamaguchi S, Taniguchi H, Kimura T and Takagi H 1998 *Phys. Rev.* B **58** R1699
[5] Moritomo Y, Takeo M, Liu X J, Akimoto T and Nakamura A 1998 *Phys. Rev.* B **58** R13334
[6] Yamaguchi S, Okimoto Y and Tokura Y 1996 *Phys. Rev.* B **54** R11022
[7] Raccah P M and Goodenough J B 1967 *Phys. Rev.* **155** 932
[8] Bose M, Ghoshray A, Basu A and Rao C N R 1982 *Phys. Rev.* B **26** 4871
[9] Señarís-Rodríguez M A and Goodenough J B 1995 *J. Solid State Chem.* **116** 224
[10] Delgado E and Michel C R 2006 *Mater. Lett.* **60** 1613
[11] Michel C R, Delgado E, Santillán G, Martínez A H and Chávez-Chávez A 2007 *Mater. Res. Bull.* **42** 84
[12] Ivanova N B, Kazak N V, Michel C R, Balaev A D and Ovchinnikov S G 2006 *Phys. Solid State* **49** 2126
[13] Pérez J, García J, Blasco J and Stankiewicz J 1998 *Phys. Rev. Lett.* **80** 2401
[14] Martínez-Juárez A, Sánchez L, Chinarro E, Recio P, Pascual C and Jurado J R 2000 *Solid State Ion.* **135** 525
[15] Suzuki T, Jasinski P, Petrovsky V, Dogan F and Anderson H U 2004 *Solid State Ion.* **175** 437
[16] Tu H Y, Takeda Y, Imanishi N and Yamamoto O 1997 *Solid State Ion.* **100** 283
[17] Battle P D and Gibb T C 1987 *J. Chem. Soc. Dalton Trans.* 667
[18] Fuertes J R, Errandonea D, Manjón F J, García D M, Segura A, Ursaki V V and Tiginyanu I M 2008 *J. Appl. Phys.* **103** 063710
[19] Guertin R P, Choi E S, Jin G B and Albrecht-Schmitt T E 2008 *J. Appl. Phys.* **103** 07B705
[20] Wang Y, Sui Y, Wang X and Su W 2009 *J. Phys.: Condens. Matter* **21** 196004
[21] Itskevich E S, Kraidenov V F and Petrova E A 2005 *Low Temp. Phys.* **31** 52
[22] Medvedeva I, Maignan A, Martin C, Bärner K, Raveau B, Bersenev Y, Mushnikov N and Gerasimov E 2005 *Physica* B **365** 114
[23] Tinte S, Rabe K M and Vanderbilt D 2003 *Phys. Rev.* B **68** 144105
[24] Moriwake H, Koyama Y, Matsunaga K, Hirayama T and Tanaka I 2008 *J. Phys.: Condens. Matter* **20** 345207
[25] Akhtar M J, Catlow C R A, Slater B, Walker A M and Woodley S M 2006 *Chem. Mater.* **18** 1552
[26] Akhtar M J and Waseem S 2001 *Chem. Phys.* **274** 109
[27] Araujo R M, Valerio M E G and Jackson R A 2008 *J. Phys.: Condens. Matter* **20** 035201
[28] Read M S D, Islam M S, Watson G W, King F and Hancock F E 2000 *J. Mater. Chem.* **10** 2298
[29] Parker S C and Price G D 1989 *Adv. Solid State Chem.* **1** 295
[30] Zhang X, Catlow C R A, Parker S C and Wall A 1992 *J. Phys. Chem. Solids* **53** 761
[31] Tang F L and Zhang X 2006 *Phys. Rev.* B **73** 144401
[32] Catlow C R A 1987 *Solid State Chemistry: Techniques* ed A K Cheetham and P Day (Oxford: Clarendon) p 231
[33] Gale J D 1996 *Phil. Mag.* B **73** 3
[34] Dick B G and Overhauser A W 1958 *Phys. Rev.* **112** 90
[35] Morris B C, Flavell W R, Mackrodt W C and Morris M A 1993 *J. Mater. Chem.* **3** 1007
[36] Mott N F and Littleton M J 1938 *Trans. Faraday. Soc.* **34** 485
[37] Gale J D 1997 *J. Chem. Soc., Faraday Trans.* **93** 629
[38] Wyckoff R W G (ed) 1964 *Crystal Structures* 2nd edn, vol 2 (New York: Wiley)
[39] Lewis G V and Catlow C R A 1985 *J. Phys. C: Solid State Phys.* **18** 1149
[40] Pérez-Cacho J, Blasco J, García J and Sanchez R 2000 *J. Solid State Chem.* **150** 145
[41] Jiang L Q, Guo J K, Liu H B, Zhu M, Zhou X, Wu P and Li C H 2006 *J. Phys. Chem. Solids* **67** 1531

[42] Moreira R L and Dias A 2007 *J. Phys. Chem. Solids* **68** 1617
[43] Zhou J-S and Goodenough J B 2005 *Phys. Rev. Lett.* **94** 065501
[44] Hwang H Y, Cheong S-W, Radaelli P G, Marezio M and Batlogg B 1995 *Phys. Rev. Lett.* **75** 914
[45] de Teresa J M, Ibarra M R, García J, Blasco J, Ritter C, Algarabel P A, Marquina C and del Moral A 1996 *Phys. Rev. Lett.* **76** 3392
[46] Liu X C, Hong R and Tian C 2009 *J. Mater Sci.; Mater. Electron.* **20** 323
[47] Goldschmidt V M 1926 *Naturwissenschaften* **14** 477
[48] Shannon R D 1976 *Acta Crystallogr.* A **32** 751
[49] Kawakami T, Nasu S, Kuzushita K, Sasaki T, Morimoto S, Yamada T, Endo S, Kawasaki S and Takano M 2003 *J. Phys. Soc. Japan* **72** 33
[50] Akhtar Z N, Akhtar M J, Clark S M and Catlow C R A 1994 *Solid State Commun.* **92** 535
[51] Xue D, Betzler K and Hesse H 2000 *J. Phys.: Condens. Matter* **12** 3113